Synthesis and dielectric evaluations of Er doped Mg-Mn-Cr ferrites

Z. H. Nawaz [a], K. M. Elhindi [b], N. Amin [a, *] , M. Akhtar [a], S. Mumtaz [c]
M. I. Arshad [a]
[a] *Department of Physics, Government College University, Faisalabad, Pakistan 38000*
[b] *Plant Production Department, College of Food & Agriculture Sciences, King Saud University, P.O. Box 2460, Riyadh 11451, Saudi Arabia*
[c] *Electrical and Biological Physics, Kwangwoon University, Seoul 01897, South Korea*

In this study solgel auto-combustion technique was successfully implanted to synthesized Er-doped soft ferrites with the chemical formula $Mg_{0.2}Mn_{0.8}Cr_{0.03}Fe_{1.97-x}Er_xO_4$ (*MMCE ferrites*). The required stoichiometric amounts of the chemicals, along with citric acid as a polymerization mediator, were calculated and used. The electrical and structural properties of Er-substituted Mg-Mn-Cr ferrite were characterized using various techniques. X-ray diffraction analysis confirmed that all samples exhibited a single-phase spinel structure with an Fd-3m space group, with X-ray density, lattice constant, and crystallite size varying based on Er concentration. Fourier Transform Infrared (FTIR) spectroscopy revealed stretching and cation vibrations of other groups in the wave number range of 250 cm^{-1} to 1500 cm^{-1}. Scanning electron microscope (SEM) images showed that the particles were agglomerated, forming larger, closely packed clusters. DC resistivity measurements indicated that the resistivity of the samples increased significantly, reaching 10^{10} Ω·m at the highest La concentration. Currently, rare-earth-substituted ferrite nanoparticles are widely used in high-frequency microwave devices due to their exceptional electrical properties, making ferrites highly valuable.

(Received September 7, 2024; Accepted November 11, 2024)

Keywords: Sol-gel, Crystalline size, Bandgap, Resistivity

1. Introduction

Over the past two decades, nanomaterials have emerged as an exciting research area, with interest growing steadily [1]. Recently, rare earth (Re) substitution improved the magnetic nanomaterials for numerous applications, including gas and moisture sensors. The type and quantity of the Re (Like Er) improved the magnetic, electric and structural properties of ferrite specimens [2-3].

Soft ferrites are chemical compounds with the formula AB_2O_4, where A and B represent divalent and trivalent metallic cations respectively, typically including iron, magnesium, manganese and erbium. Ferrites having hard and brittle nature are classified as either soft or hard due to their magnetic properties. Soft ferrites, such as those made from metals like magnesium, manganese, erbium, or chromium, have low coercivity. In contrast, magnetic materials composed of iron oxide with high concentration compare to soft ferrites and barium or strontium oxides are referred to as permanent magnets (or hard ferrites)[4]. In normal spinel ferrites, tetrahedral [A] site was occupied by divalent cations and octahedral [B] site was occupied by trivalent cations. Magnesium ferrites, $Mg^{2+}[Fe^{3+}]O_4^{2-}$, is a common example of normal ferrites. Conversely, in inverse spinel ferrites, trivalent ions $[B^{3+}]$ are equally distributed between the A and B sites while divalent ions $[A^{2+}]$ occupy octahedral sites. $CoFe_2O_4$ being a notable example for inverse spinel ferrites [5-7].

* Corresponding authors: nasir786a@yahoo.com;
https://doi.org/10.15251/JOR.2024.206.793

Spinel ferrites find applications in a range of devices, including high-density magnetic storage, switching circuits, telecommunications equipment, microwave devices, gas sensors, and magnetic fluids [8]. Ferrites exhibit insulating behavior at low temperatures but can behave as semiconductors at moderately high temperatures due to their electrical properties. Their dielectric properties make them especially useful in microwave and high-frequency devices. The electrical, magnetic, and structural properties of ferrites are heavily influenced by the synthesis method employed. Various techniques, such as sol-gel, hydrothermal, micro-emulsion, and co-precipitation methods, can be used to synthesize magnetic nanoparticles [9]. The addition of rare earth ions, such as Gd, Sm, Dy, Er, Yb, Ce, Tb, and Y, resulted in significant variations in the structural, magnetic, and electrical properties of the materials [10]

This research work aims to explore the synthesis and various characterizations of magnetic ferrites with chemical formula $Mg_{0.2}Mn_{0.8}Cr_{0.03}Fe_{1.97-x}Er_xO_4$ (MMCE ferrites) where x = 0, 0.02, 0.04, 0.06.

2. Materials and methods

For the experimental work, the following chemicals were used: $Mg(NO_3)_2 \cdot 6H_2O$, $Mn(NO_3)_2 \cdot 3H_2O$, $Er(NO_3)_3 \cdot 6H_2O$, $Fe(NO_3)_3 \cdot 9H_2O$, $Cr(NO_3)_3 \cdot 6H_2O$ citric acid, and ammonia solution. Er-doped soft ferrites with the chemical formula $Mg_{0.2}Mn_{0.8}Cr_{0.03}Fe_{1.97-x}Er_xO_4$ (MMCE ferrites) were prepared using the sol-gel auto-combustion method, with Er concentrations (x) of 0.00, 0.02, 0.04, and 0.06. Stoichiometric amounts of the nitrates of Mn, Fe, Er, Mg, and citric acid were calculated and mixed accordingly. The citric acid and metal precursors were dissolved in deionized water and stirred to get the homogeneous solution. To adjust the pH 7, ammonia solution (NH_3) was added dropwise during stirring. The solution was heated on a hot plate with magnetic stirring until a gel formed. Upon continuous heating, rapid combustion of the gel occurred, leading to the formation of an ash product. The MMCE ferrites were annealed for 3 hours at 500°C. To obtain a fine powder of MMCE ferrites, the samples were ground for 6 hours and then sintered in a furnace at 750°C for 8 hours, followed by further grinding. Afterward, the various technique were used to characterize the MMCE ferrites.

3. Result and discussion

3.1. X-Ray diffraction analysis

X-ray diffraction (XRD) is commonly used for structural analysis and phase identification. Through XRD, key structural parameters such as crystallite size, X-ray density and lattice constant are determined for MMCE ferrites. The XRD patterns for the MMCE ferrites are demonstrated in Fig. 1 (a), with diffraction angles (2θ) recorded over the range of 25° to 60°. Four distinct diffraction peaks were observed at angles 30.208°, 35.555°, 43.211°, and 57.118°, corresponding to the (220), (311), (400), and (511) planes, respectively. These peaks confirm the formation of a single-phase spinel structure with an Fd-3m space group. The peaks were further verified using the ICSD card number 73-1720. Structural parameters, including crystallite size (D), lattice constant (a), and X-ray density (d_x-ray) were calculated from the XRD data.

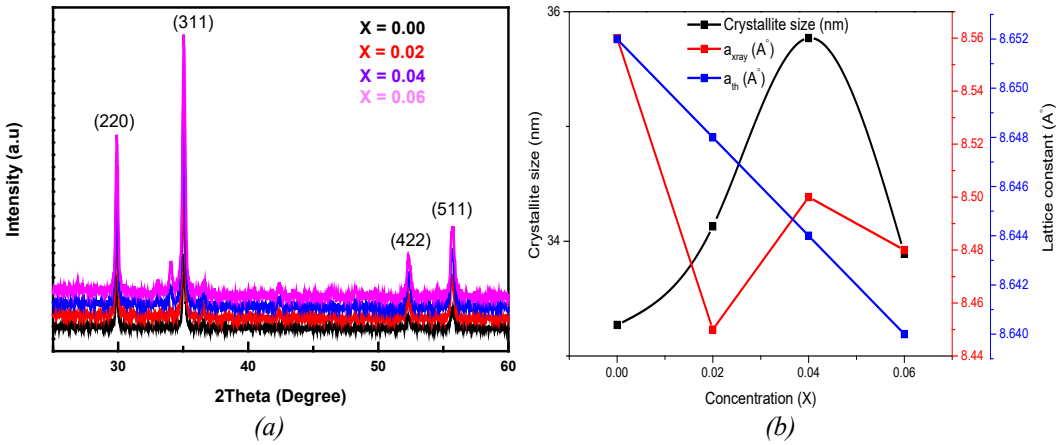

Fig. 1. a) Combined XRD pattern of MMCE ferrites, b) Crystallite size and Lattice constants (a_{exp}, a_{th}) as a function of concentration of MMCE Ferrites

The crystallite size exhibited non-linear behavior with the addition of Er^{3+}, as shown in Fig. 1 (b). The lattice constant decreased irregularly with increasing Er concentration [11]. Table 1 presents the crystallite size, X-ray density, experimental lattice parameter (a_exp), experimental volume (V), and theoretical lattice parameter (a_theo) for the MMCE Ferrites nanoparticles.

From the table, it was observed that the X-ray density (ρ) gradually increased from 4.97 to 5.19 g/cm³ with the substitution of Er^{3+} ions. These findings are consistent with results reported by Gaba S. (2018) [13]. The change in the lattice constant with Er doping can be attributed to the substitution of smaller Fe^{3+} cations (0.64 Å) with larger Er^{3+} cations (1.06 Å) [13]. Table 1 shows that the lattice constant increased irregularly, ranging from 8.3137 Å to 8.3756 Å, with the addition of Er^{3+} due to the difference in ionic radii [12]. The larger ionic radius of Er^{3+} compared to Fe^{3+} causes Er^{3+} to preferentially occupy the [B] site, leading to the expansion of the unit cell.

Table 1. Sample IDs and XRD parameters of MMCE Ferrites.

X	*D*	a_{xray} *(Å)*	a_{th} *(Å)*	*V* ($Å^3$)
0	33.27	8.56	8.652	627.22
0.02	34.13	8.45	8.648	603.35
0.04	35.77	8.5	8.644	614.12
0.06	33.89	8.48	8.64	609.80

3.2. UV–visible spectroscopy

The optical band gap of the MMCE ferrites was determined using UV-Vis spectroscopy, as shown in Figure 2. The ferrite powders from all samples with identical concentrations were dissolved in water to examine their optical band gaps. The influence of Er on the ferrites was investigated, with the minimum band gap of 2.81 eV observed for Er = 0.06. The variation in band gap was attributed to factors such as grain size, impurity centers, lattice constant, and surface smoothness.

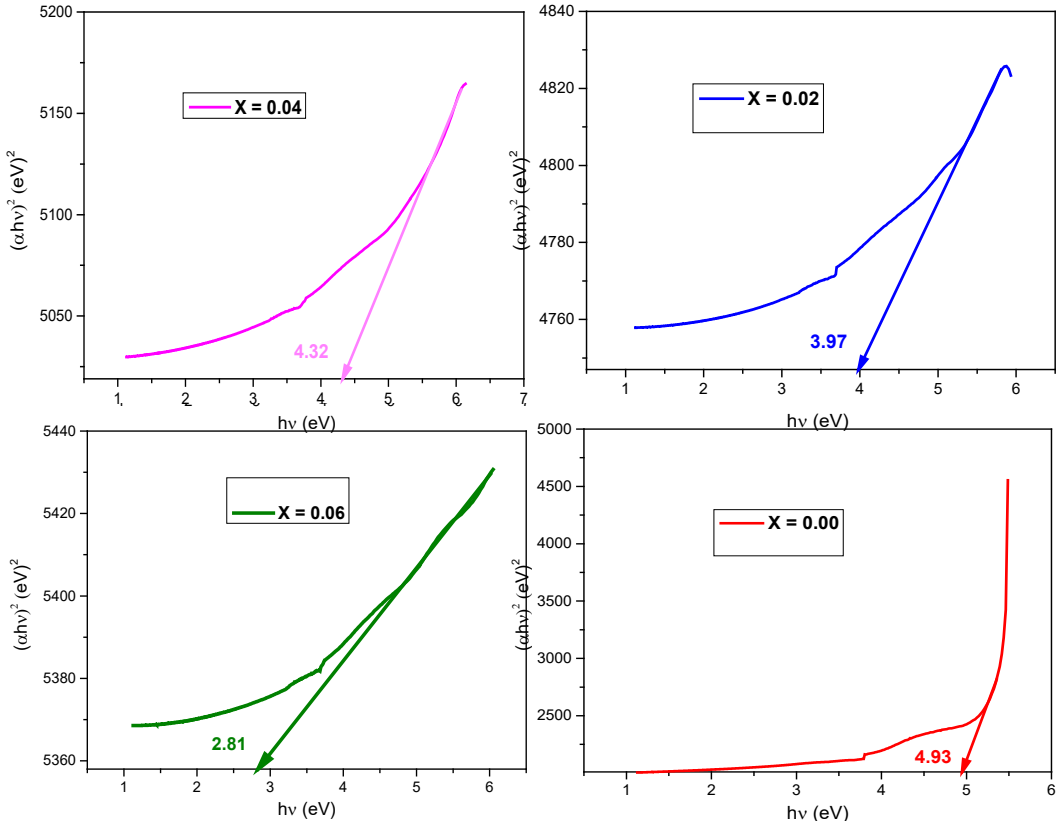

Fig. 2. Pattern of UV vis spectroscopy of MMCE ferrites.

3.2. SEM Analysis

Microstructural analysis of the MMCE ferrites was carried out using scanning electron microscopy (SEM). The SEM images and corresponding grain size values for MMCE Ferrites, as determined from the micrographs, are shown in Fig. 5. The images reveal that the particles are agglomerated, forming larger clusters, and that the particles are closely packed.

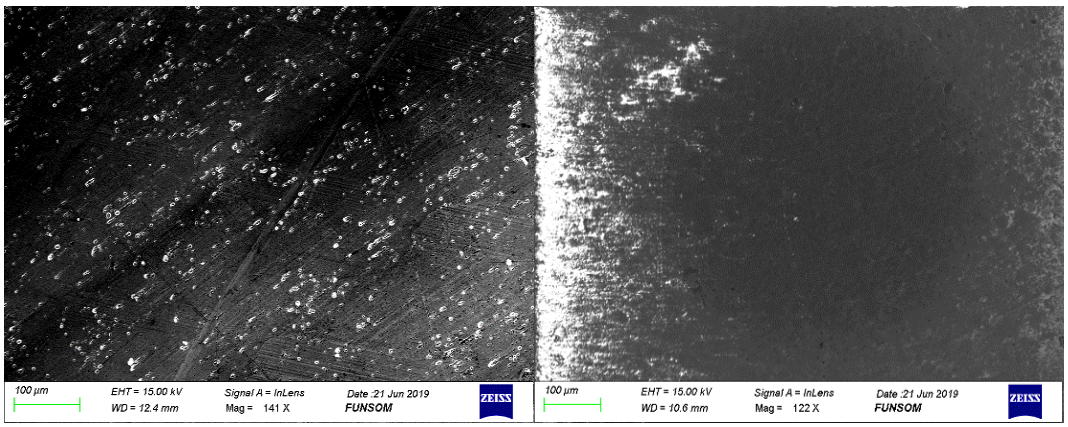

(a) *(b)*

Fig. 3. SEM micrographs of MMCE ferrites.

3.4. FTIR analysis

FTIR spectroscopy is a highly effective technique for confirming structural parameters in synthesized MMCE nanoferrites. It provides valuable insights into the vibrational and structural

modes of the materials [13]. The FTIR spectra of Er-doped MMC ferrite nanoparticles were recorded in the wavenumber range of 250 cm^{-1} to 3500 cm^{-1}, confirming the formation of spinel ferrite. The IR spectra discovered two major absorption bands, characteristic of the material, along with peaks associated with the presence of water [14].

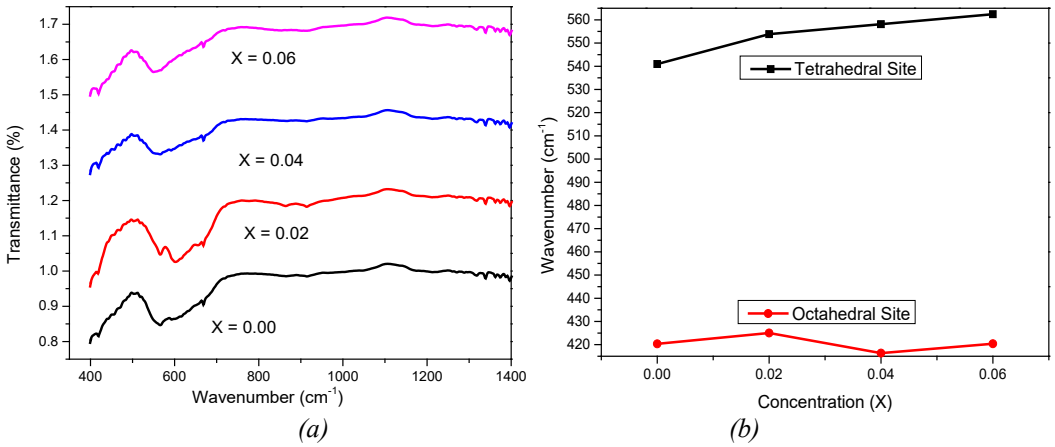

Fig. 4. FTIR spectrum of MMCE ferrites.

Figure 4 shows the absorption spectra of the ferrite samples. Typically, ferrite IR spectra consist of two prominent absorption bands. The higher wavenumber absorption band (υ_1) at 537.307 cm^{-1} is attributed to the stretching vibration of the Mg, or Mn-oxygen bond at the tetrahedral (A) site. The lower wavenumber absorption band (υ_2), observed between 417.08 cm^{-1} and 417.97 cm^{-1}, corresponds to the stretching vibration of the Fe, Cr, or Er-oxygen bond at the octahedral (B) site.

The data shows a slight shift in the wavenumber at the octahedral (B) site from higher to lower frequencies, attributed to the substitution of Er ions. Er has a larger ionic radius compared to iron and a greater mass than other cations, which leads to this shift [15]. Additionally, a stretching vibration of the O-H bond was observed at 3400 cm^{-1} [16], while the band between 1400 cm^{-1} and 1550 cm^{-1} indicated the presence of CO_2 molecules absorbed from the atmosphere [17]. A band around 2300 cm^{-1} was associated with the asymmetric carboxyl group. The two absorption bands, υ_1 and υ_2, exhibit different frequencies due to the variation in bond lengths at the tetrahedral and octahedral sites.

Table 2. Vibrational bonds of MMCE ferrites.

X	*Tetrahedral Site*	*Octahedral*
0	540.95	420.35
0.02	553.83	425.04
0.04	558.12	416.36
0.06	562.41	420.39

3.5. Current voltage analysis

A Keithley electrometer model 22401 was used for electrical measurements of MMCE nanoferrites, specifically employing current-voltage (I-V) analysis. Silver paste was applied to the MMCE ferrite pellets to ensure fine ohmic contact. The electrical properties investigated include the calculation of electrical resistivity. In the Er-substituted MMCE Ferrites materials synthesized in this study, DC resistivity was measured using a two-probe system within a temperature range of 300–750 K.

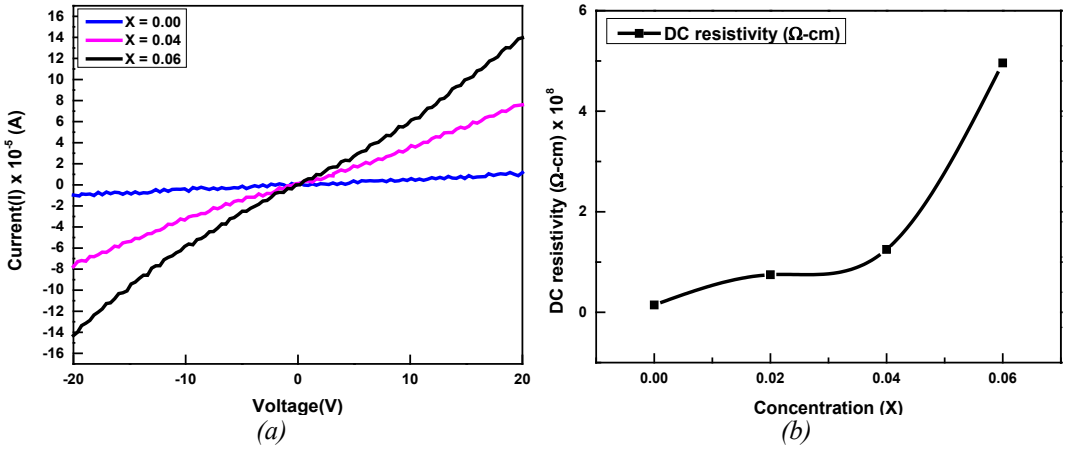

Fig. 5. Graph of log ρ vs. T of MMCE soft ferrites.

The DC resistivity for each MMCE ferrite was premeditated from the resistance and dimensions of the pellets using the formula: ρ = R. A/L, where A is the cross-sectional area of the MMCEF pellets, R is the resistance, and L is the thickness of the pellet[18-20]. Fig. 3 presents a graph of electrical resistivity (ρ) versus Curie temperature (T) for the MMCE nanoferrites. The temperature at which the resistivity reaches its maximum value is defined as the Curie temperature. The graph illustrates how electrical resistivity varies with temperature.

Additionally, the variation of log ρ with 1000/T (K^{-1}) for MMCE nanoferrites is shown in Fig. 5. The resistivity decreases with increasing temperature, following the Arrhenius relation: $\rho=\rho_0 \cdot e^{\Delta E/kBT}$, where ΔE is the activation energy required to transfer an electron from one ion to another, ρ_0 is a temperature-independent constant, T is the temperature in Kelvin, and k_B is the Boltzmann constant. From the graph, it is observed that the resistivity of MMCE Ferrites increases with the concentration of Er. It was noted that as the erbium content increased, resistivity also increased at various temperatures. The graph also depicts the relationship between Er concentration and activation energy. Initially, activation energy decreases with increasing Er concentration; however, when the Er concentration reaches 0.037, the activation energy decreases maximum, and increases with further increases in Er concentration.

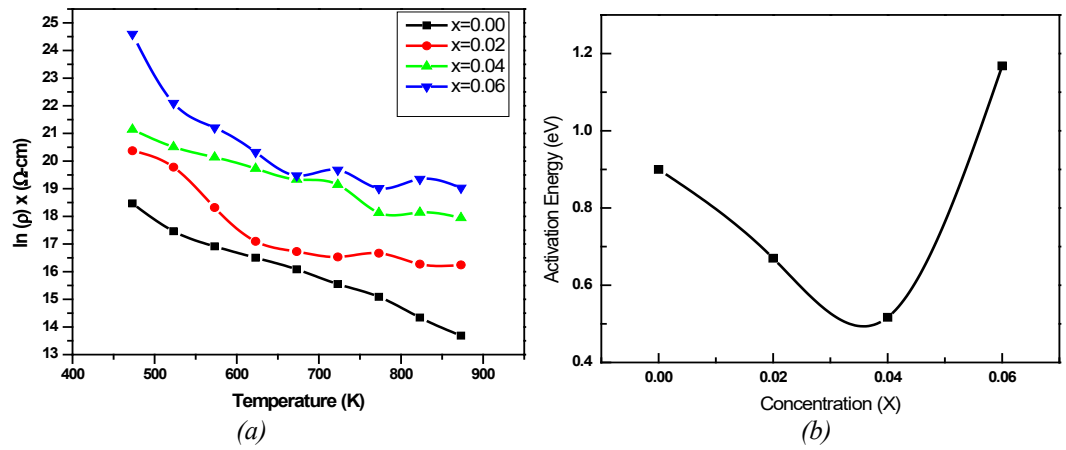

Fig. 6. Graph of T vs log ρ of MMCE soft ferrites.

3.6. Dielectric analysis

Electrical dipoles are generated in spinel materials, influencing their dielectric properties. The distinction in dielectric constant (ε′) with log frequency (log f) is illustrated in Figures 7. The results indicate that as the concentration of Er^{3+} increases, the dielectric constant shows a decreasing trend with frequency. This variation in dielectric properties is influenced by factors such as synthetic methods, frequency, temperature, stoichiometry, and crystallite size.

The dielectric behavior is primarily attributed to charge hopping and polarization. At lower frequencies, hopping between Fe^{3+} and Fe^{2+} cations at octahedral sites occurs more easily, resulting in higher dielectric constant values. As the frequency increases, the hopping becomes more tough due to the alternating nature of the applied frequency, causing a reduction in the dielectric constant. Another factor contributing to dielectric dispersion is the polarization of charges, which predominantly occurs at the grain boundaries. At higher frequencies, polarization takes place within smaller grain boundaries.

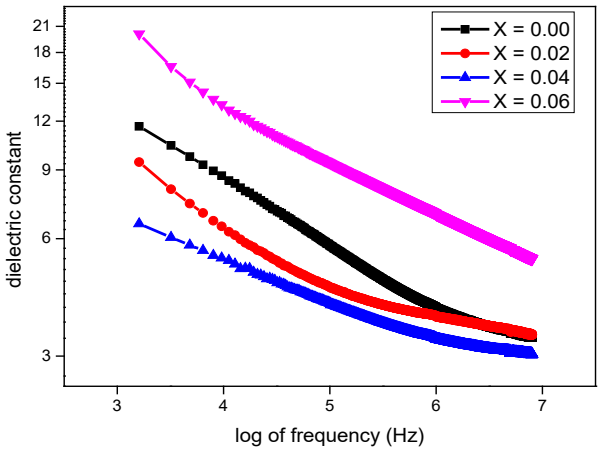

Fig. 7. FTIR spectrum of MMCE ferrites

3.7. Magnetic analysis

The magnetic behavior of Er-doped MMC-soft ferrites is illustrated in Fig. 9 at room temperature. The hysteresis loops for all the ferrites show similar magnetic characteristics. Hysteresis loops are used to measure various magnetic parameters, including, coercivity (H_c), saturation magnetization (M_s) and remanence magnetization (M_r), [3, 57], as reported in Table 6. The saturation magnetization (M_s) exhibits a variable trend with increasing Er^{3+} concentration. This variability is attributed to the presence of anomalous factors and secondary phases [21]. Similarly, coercivity (H_c) also shows variability with increasing Er^{3+} cations, as detailed in Table 6. The minimum values of remanence and saturation magnetization are observed at x = 0.06, with values of 71.33 emu/g and 21.57 emu/g, respectively. The magnetic properties of MMCE ferrites are influenced by factors such as synthesis technique, grain size, and cation distribution.

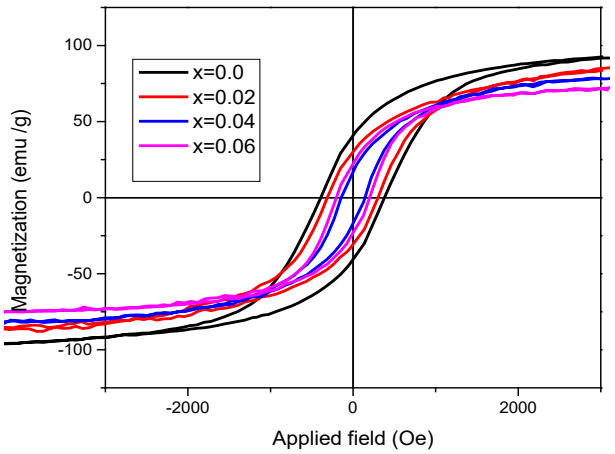

Fig. 8. M-H loops of MMCE ferrites.

Table 3. Magnetic parameters of MMCE ferrites.

X	Ms	Hc	Mr
0.00	91.87	393.21	40.98
0.02	83.98	321.72	29.89
0.04	77.37	142.98	16.03
0.06	71.33	214.48	21.57

4. Conclusion

The present study investigates the effect of Er substitution in MMC Ferrites. All samples were characterized using various techniques, including SEM, FTIR, XRD, UV-Vis Spectroscopy, Current-Voltage (I-V) measurements, and Raman Spectroscopy. The XRD results indicate a single-phase spinel structure with particle sizes ranging from 33.27 to 35.77 nm and lattice parameters varying from 8.64 to 8.652 Å. FTIR analysis confirms the cation distribution and the presence of bonds characteristic of the spinel structure, with peaks in the wavenumber range of 416 cm^{-1} to 553 cm^{-1}, consistent with spinel ferrites. UV-Vis spectroscopy reveals a band gap energy range of 2.8 to 4.9 eV. Raman spectroscopy identifies five distinct Raman peaks, each corresponding to specific Raman modes. I-V measurements show that resistivity increases with temperature. Additionally, the dielectric constant diminutions with higher Er concentration and frequency. The saturation magnetization decreases with the addition of Er, with the minimum value observed at a Er concentration of 0.06. Based on these results, the materials studied are deemed appropriate for high-frequency applications.

Funding

Researchers Supporting Project number (RSPD2024R952), King Saud University

Acknowledgements

The authors extend their deep appreciation to Researchers Supporting Project number (RSPD2024R952), King Saud University, Riyadh, Saudi Arabia.

References

[1] A.U. Rehman, G. Abbas, B. Ayoub, N. Amin, M.A. un Nabi, N.A. Morley, M. Akhtar, M.I. Arshad, M.U. Khalid, M. Afzaal, Materials Science and Engineering: B 291 (2023) 116407; https://doi.org/10.1016/j.mseb.2023.116407

[2] K. Hussain, N. Amin, M.I. Arshad, Ceramics International, 47 (2021) 3401-3410; https://doi.org/10.1016/j.ceramint.2020.09.185

[3] Z. Latif, A. Rehman, M. Yusuf, N. Amina, M. Arshad, Journal of Ovonic Research, 18 (2022) 627-635; https://doi.org/10.15251/JOR.2022.184.627

[4] K. Mehmood, A.U. Rehman, N. Amin, N. Morley, M.I. Arshad, Journal of Alloys and Compounds, 930 (2023) 167335; https://doi.org/10.1016/j.jallcom.2022.167335

[5] M. Akram, S. Akhlaq, M.I. Arshad, N. Amin, A.A. Ifseisi, M. Akhtar, N.T.K. Thanh, N. Morley, S. Sadiq, S. Hussain, Solid State Communications, 373 (2023) 115317; https://doi.org/10.1016/j.ssc.2023.115317

[6] N. Amin, M. Akhtar, M. Sabir, K. Mahmood, A. ALIa, G. Mustafa, M. Hasan, A. Bibi, M. Iqbal, F. Iqbal, Synthesis, Structural and Optical Properties of Zn-Substituted Co W-Ferrites By Coprecipitation Method, 16 (2020) 11-19.

[7] A. Aslam, A. Razzaq, S. Naz, N. Amin, M.I. Arshad, M.A.U. Nabi, A. Nawaz, K. Mahmood, A. Bibi, F. Iqbal, Journal of Superconductivity and Novel Magnetism (2021) 1-10; https://doi.org/10.1007/s10948-021-05802-4

[8] G. Abbas, A.U. Rehman, W. Gull, M. Afzaal, N. Amin, L. Ben Farhat, M. Amami, N.A. Morley, M. Akhtar, M.I. Arshad, Journal of Sol-Gel Science and Technology 101(2) (2022) 428-442; https://doi.org/10.1007/s10971-021-05713-9

[9] M.I.U. Haq, A.u. Rehman, M. Asghar, M.A.U. Nabi, N. Amin, S. Tahir, M.I. Arshad, Journal of Superconductivity and Novel Magnetism 35(3) (2022) 719-732; https://doi.org/10.1007/s10948-021-06124-1

[10] A. Aslam, A.U. Rehman, N. Amin, M. Amman, M. Akhtar, N. Morley, M.S. Al-Sharif, M. Hessien, K.A. El-Nagdy, M.I. Arshad, Materials Chemistry and Physics 294 (2023) 127034; https://doi.org/10.1016/j.matchemphys.2022.127034

[11] A.U. Rehman, N. Morley, N. Amin, M.I. Arshad, M.A. un Nabi, K. Mahmood, A. Ali, A. Aslam, A. Bibi, M.Z. Iqbal, Ceramics International 46(18) (2020) 29297-29308; https://doi.org/10.1016/j.ceramint.2020.08.106

[12] A. Aslam, A.U. Rehman, N. Amin, M. Amami, M. Nabi, H. Alrobei, M. Asghar, N. Morley, M. Akhtar, M.I. Arshad, Journal of Superconductivity and Novel Magnetism (2021) 1-11; https://doi.org/10.1007/s10948-021-06085-5

[13] N. Amin, A. Razaq, A.U. Rehman, K. Hussain, M.A.U. Nabi, N. Morley, M. Amami, A. Bibi, M.I. Arshad, K. Mahmood, Journal of Superconductivity and Novel Magnetism 34 (2021) 2945-2955; https://doi.org/10.1007/s10948-021-06053-z

[14] N. Amin, M.S.U. Hasan, Z. Majeed, Z. Latif, M.A. un Nabi, K. Mahmood, A. Ali, K. Mehmood, M. Fatima, M. Akhtar, Ceramics International 46(13) (2020) 20798-20809; https://doi.org/10.1016/j.ceramint.2020.05.079

[15] M.I. Arshad, M. Hasan, A.U. Rehman, M. Akhtar, N. Amin, K. Mahmood, A. Ali, T. Trakoolwilaiwan, N.T.K. Thanh, Ceramics International 48(10) (2022) 14246-14260; https://doi.org/10.1016/j.ceramint.2022.01.313

[16] A.U. Rehman, N. Amin, M.B. Tahir, M.A. un Nabi, N. Morley, M. Alzaid, M. Amami, M. Akhtar, M.I. Arshad, Materials Chemistry and Physics 275 (2022) 125301; https://doi.org/10.1016/j.matchemphys.2021.125301

[17] A.U. Rehman, S. Sharif, H. Hegazy, N. Morley, N. Amin, M. Akhtar, M.I. Arshad, Z. Farooq, Z. Munir, T. Munir, Materials Today Communications (2023) 105371; https://doi.org/10.1016/j.mtcomm.2023.105371

[18] A. Aslam, A.U. Rehman, N. Amin, M. Amami, M. Nabi, H. Alrobei, M. Asghar, N. Morley,

M. Akhtar, M.I. Arshad, Journal of Superconductivity and Novel Magnetism (2021) 1-11; https://doi.org/10.1007/s10948-021-06085-5

[19] G. Hussain, I. Ahmed, A.U. Rehman, M.U. Subhani, N. Morley, M. Akhtar, M.I. Arshad, H. Anwar, Journal of Alloys and Compounds (2022) 165743; https://doi.org/10.1016/j.jallcom.2022.165743

[20] I. ALI, N. Amin, A. Rehman, M. Akhtar, M. Fatima, K. Mahmood, A. ALIa, G. Mustafa, M. Hasan, A. Bibi, Digest Journal of Nanomaterials and Biostructures 15(1) (2020).

[21] A. Aslam, A.U. Rehman, N. Amin, M.A. un Nabi, Q. ul ain Abdullah, N. Morley, M.I. Arshad, H.T. Ali, M. Yusuf, Z. Latif, Journal of Physics and Chemistry of Solids 154 (2021) 110080; https://doi.org/10.1016/j.jpcs.2021.110080